Tunable Topological Acoustic Tamm States in Comblike Structures Based on Band Inversion around Flat Bands

Soufyane Khattou, Yamina Rezzouk, Madiha Amrani, Mohamed El Ghafiani, El Houssaine El Boudouti, Abdelkrim Talbi, Bahram Djafari-Rouhani

crystals

MDPI

Article

Tunable Topological Acoustic Tamm States in Comblike Structures Based on Band Inversion around Flat Bands

Soufyane Khattou [1], Yamina Rezzouk [1], Madiha Amrani [1], Mohamed El Ghafiani [1], El Houssaine El Boudouti [1,*], Abdelkrim Talbi [2] and Bahram Djafari-Rouhani [3]

[1] LPMR, Département de Physique, Faculté des Sciences, Université Mohammed I, Oujda 60000, Morocco
[2] Univ. Lille, CNRS, Centrale Lille, Université Polytechnique Hauts-de-France, UMR 8520-IEMN, LIA LICS, 59000 Lille, France
[3] Institut d'Electronique, de Microélectronique et de Nanotechnologie (IEMN), UMR CNRS 8520, Département de Physique, Université de Lille, 59655 Villeneuve d'Ascq, France
* Correspondence: e.elboudouti@ump.ac.ma

Abstract: We investigate the existence of acoustic Tamm states at the interface between two one-dimensional (1D) comblike phononic crystals (PnCs) based on slender tubes and discuss their topological or trivial character. The PnCs consist of stubs grafted periodically along a waveguide and the two crystals differ by their geometrical parameters (period and length of the stubs). We use several approaches to discuss the existence of Tamm states and their topology when connecting two half-crystals. First, we derive a necessary and sufficient condition on the existence of interface states based on the analysis of the bulk band structure and the symmetry of the band edge states. This approach is equivalent to an analysis of the Zak phases of the bulk bands in the two crystals. Indeed, a topological interface state should necessarily exist in any common bandgap of the two PnCs for which the lower (upper) band edges have opposite symmetries. A novelty of our structure consists in the fact that the symmetry inversion results from a band closure (flat band) rather than from a gap closure, in contrast to previous works. Then, such interface states are revealed through different physical quantities, namely: (i) the local density of states (LDOS), which exhibits a high localization around the interface; (ii) sharp peaks in the transmission spectra in the common bandgap when two finite crystals are connected together; (iii) the phases of the reflection coefficients at the boundary of each PnC with a waveguide, which have a direct relationship with the Zak phases. In addition, we show that the interface states can transform to bound states in the continuum (BICs). These BICs are induced by the cavity separating both PnCs and they remain robust to any geometrical disorder induced by the stubs and segments around this cavity. Finally, we show the impossibility of interface states between two connected PnCs with different stub lengths and similar periods. The sensitivity of these states to interface perturbations can find many practical applications in PnC sensors.

Keywords: topological interface states; phononic crystals; comblike structure; Zak phase

Citation: Khattou, S.; Rezzouk, Y.; Amrani, M.; El Ghafiani, M.; El Boudouti, E.H.; Talbi, A.; Djafari-Rouhani, B. Tunable Topological Acoustic Tamm States in Comblike Structures Based on Band Inversion around Flat Bands. *Crystals* **2022**, *12*, 1685. https://doi.org/10.3390/cryst12121685

Academic Editors: Jin-Chen Hsu and Jia-Hong Sun

Received: 30 September 2022
Accepted: 15 November 2022
Published: 22 November 2022

1. Introduction

Phononic crystals (PnCs) are artificial periodic devices used for controlling and manipulating sound and elastic waves [1–3] in analogy with electromagnetic waves in photonic crystals and electron wave functions in semiconductors [4]. Of particular interest, one-dimensional (1D) periodic systems based on slender tubes have been studied to design band-gap materials [5,6] with potential applications for controlling noise, filtering, sensing, demultiplexing and acoustic metamaterials with negative modulus [7–10]. Within this field, several devices have been proposed to achieve transmission gaps and filters such as Helmholtz resonators [11,12], asymmetric loops [13] and side-coupled stubs [5,6]. Additionally, breaking the periodicity of the perfect phononic crystal by a defect may give rise to localized defect modes within the forbidden gaps [14]. Particularly, great interest has been paid to localized surface modes called Tamm states [15], which were originally discovered

for electrons in condensed matter physics. Later, Tamm states have been extended to classical wave systems such as acoustics [16–18], photonics [19–21] and plasmonics [22].

In recent years, several studies have been devoted to investigate the existence of interface Tamm states based on the topological properties of band structures in the considered artificial materials that can be revealed through the Berry phase approach [23]. In 1D periodic systems, the topology of the bands is characterized by the concept of Zak phase, a special kind of Berry phase [24–28]. Recently, topological interface states and Zak phase have been extended to various branches of physics such as photonics [26,29–34], plasmonics [22,35], acoustics and mechanical systems [36–39] and metamaterials [40,41]. The topological invariant has been successfully applied to predict the existence of interface states from the Zak phases of bulk bands. The Zak phase of each bulk band is calculated from different approaches such as: the symmetry of the band-edge states [42] or a condition on the sign of the phase of the reflection coefficient at the termination of the periodic structure [26,32].

Topological interface states have been the subject of a great interest in acoustic wave systems. Meng et al. [43] and Xiao et al. [27] showed interface states in phononic crystals based on cylindrical waveguides with periodically alternating cross-sectional areas. To et al. [44] studied the existence of acoustic interfacial waves in multilayers. However, few works [42,45] have been devoted to study interface states in periodic acoustic systems based on locally grafted resonators or stubs. Generally, the previous studies are based on 1D dimerized devices described by the Su–Schrieffer–Heeger (SSH) model [46–49] and the bandgap inversion process with topological transition points. However, in this work, we use a very different approach from the SSH model which is based on the band inversion around flat bands and show that a unit cell with only one stub is sufficient to introduce topological Tamm states at the interface between two PnC systems (Figure 1). In contrast to previous works, the symmetry inversion in our structure results from a band closure rather than the bandgap closure. First, we show the possibility of existence of interface states between two comblike structures through an analysis of the bulk band structure and the symmetry of the band edge states. This approach is equivalent to the analysis of the Zak phases of the bulk bands in the two PnCs. The Zak phase of each band is calculated both directly from its definition based on a double integration over the Brillouin zone and the unit cell (Equation (2) of the paper), or from the symmetry of the band-edge states. Indeed, we show the existence of a topological interface state inside the common bandgap of two PnCs for which the lower (or upper) band edges have opposite symmetries. Then, we show that such interface states can be revealed by an analysis of the local density of states (LDOS) at the interface between two semi-infinite PnCs (Figure 1a). Furthermore, we confirm the existence of such topological interface states by several arguments, namely, a reflection phase condition and transmission spectra. When two finite periodic systems are connected together, the Tamm states are revealed by asymmetrical sharp peaks in the shape of Fano resonances [50] in the transmission spectra inside the common bandgaps (Figure 1c). These modes can become topological bound states in the continuum (BICs) with infinite quality factor [51] for some geometrical parameters. These BICs are induced by the cavity separating both PnCs and remain robust to any geometrical perturbation in the stubs and segments around this cavity. Moreover, in addition to true localized Tamm states that fall inside the common bandgaps of two PnCs, we discuss the existence of semilocalized interface states, which appear as well-defined resonances within the bandgap of one PnC and the bulk band of the other one. Finally, we show the impossibility of interface states between two PnCs with different stub lengths and similar periods. The analytical calculations developed here are performed by means of the Green's function approach [3,52]. It is worth noticing that the interface states predicted here can be observed experimentally in the low-frequency domain using slender tubes or Helmholtz resonators as in the experiments based on the impulse response technique [12,14,53–55].

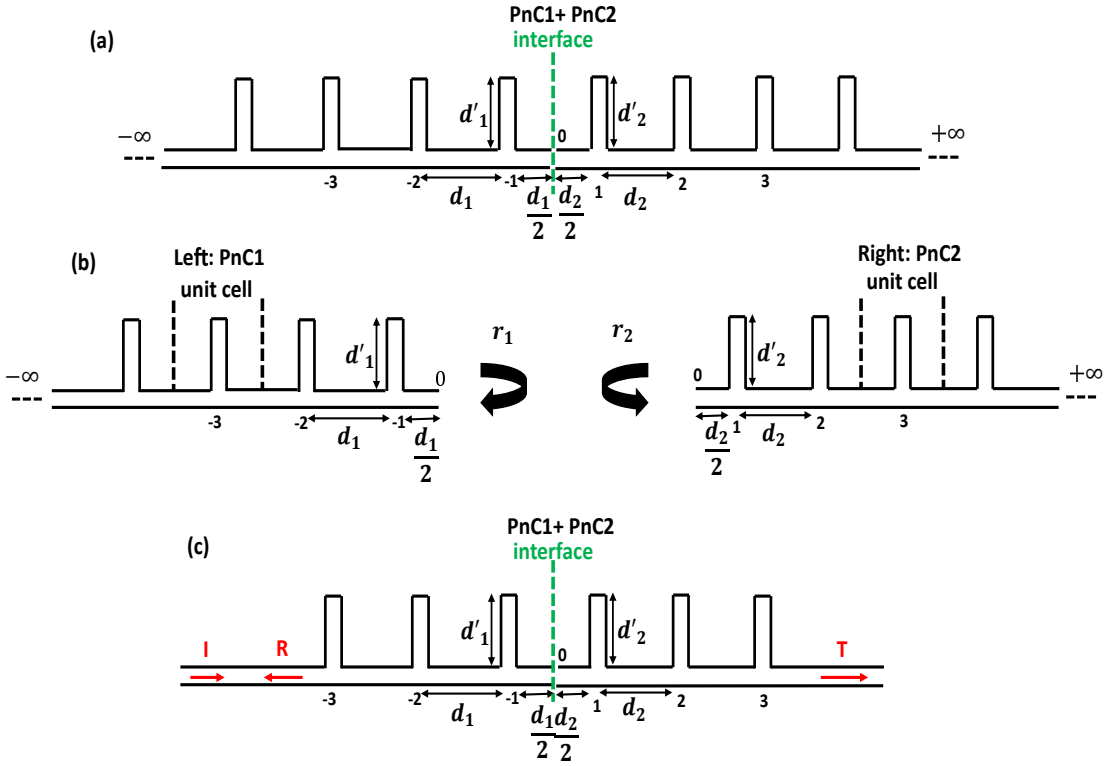

Figure 1. (**a**) Interface between two semi-infinite PnCs terminated by segments of lengths $\frac{d_1}{2}$ and $\frac{d_2}{2}$. Each PnC is composed of one stub by period. (**b**) Semi-infinite PnCs (the first PnC in the left and the second one in the right) in contact with a waveguide. r_1 and r_2 are the reflection coefficients for the PnC1 and PnC2, respectively. (**c**) Interface between two finite PnCs each one composed of 3 cells. I, R and T denote the incident, reflected and transmitted acoustic waves, respectively.

The outline of this paper is as follows: In Section 2, we discuss the possibility of the existence of acoustical Tamm states from the band structures and Zak phases of the bulk bands of periodic infinite PnCs. In Section 3, we show the interface states through the analysis of the dispersion relation and LDOS spectra of two semi-infinite PnCs (Figure 1c). In Section 4, we prove the existence of interface states from reflection phases and the transmission coefficient. In Section 5, we give a conclusion for this work.

2. Interface States from Zak Phases and Symmetry of Edge Modes

The PnC device considered here is a 1D periodic system consisting of alternating stubs grafted periodically along a waveguide (Figure 1). The tubes and waveguides are filled with the same fluid (air) and characterized by the same impedance $Z = \frac{\rho v}{a}$, where $\rho = 1.2$ kg/m^3 is the mass density of air, $v = 342$ m/s is the longitudinal speed of acoustic wave and $a = 3.14$ cm^2 is the cross section of the guide [53]. The PnCs are made by the same material (air) with different geometrical parameters: the first PnC (on the left-hand side) is made by stubs of length d'_1 and a period of length d_1 with a tube of length $\frac{d_1}{2}$ at the surface, whereas the second PnC (on the right-hand side) is made by stubs of length d'_2 and a period of length d_2 with a tube of length $\frac{d_2}{2}$ at the surface (Figure 1b). The Dirichlet boundary condition is applied at the end of stubs, which means closed stubs yielding the vanishing of the velocity or of the derivative of the pressure field. It should be pointed out that the validity of our results is subject to the requirement that the propagation is monomode, i.e., the cross section of the slender tubes is supposed to be much smaller than their length and the propagation wavelength λ ($\sqrt{a} << d_i, \lambda$).

The dispersion relation of an infinite comblike PnC structure, composed of stubs of length d'_i and separated from each other by the period d_i, is given by [5]

$$\cos(k_B^i d_i) = C_i + \frac{1}{2}\frac{S_i C_i'}{S_i'}, \tag{1}$$

where $C_i = \cos(kd_i)$, $S_i = -j\sin(kd_i)$, $C_i' = \cos(kd_i')$ and $S_i' = -j\sin(kd_i')$ $(i = 1, 2)$. $k = \frac{\omega}{v}$ is the wave-vector of the acoustic wave in the slender tubes and $j = \sqrt{-1}$. ω is the angular frequency.

The Zak phase is a special type of Berry phase in 1D periodic systems. It is defined for the nth band by [26,27]

$$\theta_n^{\text{Zak}} = \int_{-\pi/d_1}^{\pi/d_1} \left[i \int_{\text{unit cell}} \frac{1}{2\rho v^2} dx u_{n,q}^*(x) \partial_q u_{n,q}(x) \right] dq, \tag{2}$$

where x represents the spatial coordinate and $u_{n,q}$ is the Bloch wave eigenfunction with a given wave vector q. For the nth band of a 1D PnC, the pressure field is defined as $p_{q;n,q}(x) = u_{n,q}(x)\exp(iqx)$. The quantity $\frac{1}{2\rho v^2}$ is the weight function of an acoustic system.

Although the Zak phase of a given band can be calculated analytically from the knowledge of the Bloch eigenfunctions, it can also be determined from the symmetry of the band-edge states. If the unit cell admits an inversion symmetry and the origin of the coordinates is fixed at the symmetry center, the Zak phase calculated from Equation (2) can take only two defined values, 0 or π [26,32,42]. If the wave field at the edges of the selected band has identical symmetry, meaning both are symmetric or antisymmetric, then the Zak phase of this band is zero. Otherwise, the Zak phase is π.

To demonstrate the topological properties in our PnC structure, we consider first an infinite comblike structure composed by stubs of length $d_1' = 10$ cm and a period of length d_1 variable (Figure 1). We should note here that our unit cell contains only one stub, in contrast to what has been studied in the literature, where authors have considered dimerized unit cells made of two stubs by unit cell [25–27,29]. In the latter, the band gaps can close and reopen by changing the period of the system. Our proposal is, in contrast to such systems, based on the acoustic analogue of the SSH model [42,45–49] with dimerized unit cells. Indeed, the symmetry inversion in our PnC structure results from a band closure rather than from a gap closure. The advantage of our proposed approach lies in the fact that the gaps around the flat bands are hybridization gaps where the imaginary part of the wave vector takes very high values and consequently the interface mode becomes very localized. However, in more common cases where the final gap is obtained by leaving the degeneracy of a closed gap (as, for instance, in the SSH model), this gap is of Bragg type and the interface states may be less localized. In addition, our system may present a topological BIC induced by the cavity separating the two PnCs. This BIC remains robust under any geometrical perturbation in the stubs and segments around this cavity.

Figure 2 shows the bandgap structure of an infinite comblike PnC composed by stubs of length $d_1' = 10$ cm as a function of the period of length d_1. The bandgaps of the comblike structure originate either from the periodicity of the crystal (Bragg gaps) or from local resonant states induced by the grafted stubs (hybridization gaps). One can notice the existence of band crossing points (labeled 1–6 by green circles) that represent the situation where the dispersion curve becomes totally flat (without dispersion) and the widths of the corresponding passbands vanish. By changing the parameter d_1, the bands close and reopen at these points. The edge modes of two bands in the vicinity of a flat band are characterized by the same symmetry. The symmetric and antisymmetric band edge states as a function of d_1 are indicated by pink and cyan colors, respectively. As a function of d_1, the Zak phase is zero if the band edge states are characterized by the same symmetry, otherwise the Zak phase is π. The gray color represents areas where the Zak phase is π, while the dark cyan color indicates areas where the Zak phase is 0.

Now, two PnCs with different values of d_1 near a band crossing point can exhibit a common bandgap such that the symmetries of the upper band edge state for the first

PnC and the lower band edge state for the second PnC are the same (see the vertical dashed lines and encircled area in Figure 2 for some selected values of d_1). This property is sufficient to ensure that the common gap can support a topological interface state. It is shown [26] that it is sufficient to look at the symmetry of the lower (or upper) band edges of a common bandgap to know if it supports an interface state or not. For example, consider two phononic crystals labeled PnC1 and PnC2 in Figure 2 for $d_1 = 2$ cm and $d_2 = 7$ cm, respectively. One can see that around the crossing bands noted 3 at 3429 Hz, the two PnCs present a common gap (indicated by large circles) and the symmetry of the upper edge mode of PnC1 is similar to the symmetry of the lower edge mode of PnC2 (this is shown in more detail in the following). A similar analysis can be done for PnC2 and PnC3 around point 4 and PnC1 and PnC3 (or PnC4) around point 1, etc. It can be noticed that it is preferable to not chose both PnCs very close to the same crossing point, because in that case, the common bandgap between the two PnCs becomes very narrow and the topological interface state will appear very close to the passbands. Figure 2 gives us a clear idea on how the two PnCs should be chosen before coupling them to achieve a common bandgap that can support an interface state in a broad bandgap. Generally, the existence of topological interface states is analyzed on the basis of the gap closure process in the framework of the SSH model [27,29]; here, we provide another approach based essentially on the band closure mechanism around flat bands. An analysis of the possibility of topological Tamm states for the four PnCs shown in Figure 2 is discussed in detail below.

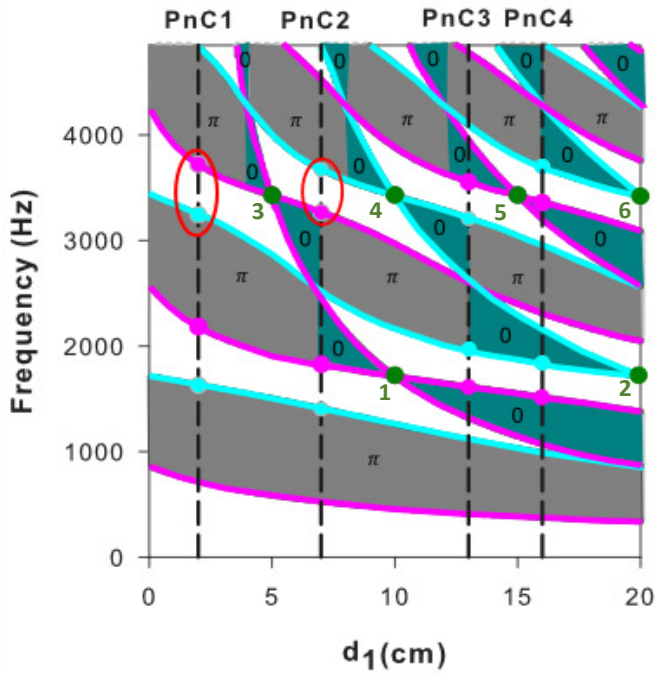

Figure 2. Bandgaps (white area) separated by bands (shaded area) of an infinite PnC as a function of d_1, while d_1' is fixed at 10 cm. The green circles labeled 1 to 6 indicate the positions of the band crossing points (where the dispersion curves become flat). The vertical dashed lines correspond to the four PnCs discussed in Figure 3. Pink and cyan colors indicate the symmetric and antisymmetric edge modes of the common bandgaps, respectively. The bands with π and 0 Zak phases are indicated by gray and dark cyan colors, respectively.

Indeed, in order to give a better idea about the possible combinations of PnCs that can display interface states, we provide in Figure 3a–d, four examples of band structures (frequency as a function of dimensionless Bloch wave vector $k_B^1 d_1$) of infinite PnCs, indicated by vertical lines in Figure 2 for four values of the period d_1. Let us notice that in these band structures, the lowest dispersion curve displays a cut-off frequency that is a result of the boundary condition at the end of stubs which are closed tubes. This is useful

in the determination of their Zak phases from the symmetry of the band edge states. To identify the Zak phase of each bulk band, we use either the integral in Equation (2) or the symmetry of the acoustic pressure field at the band edge states. The Zak phase is π if the band edge states of a given band have opposite symmetries with respect to the symmetry plane of the unit cell. Otherwise, the Zak phase is zero if the band edge states have the same symmetry (i.e., both symmetric or both antisymmetric). The Zak phase of each bulk band is denoted π or zero in black in (a)–(d). The pink (cyan) dots at the band edges represent the symmetric (antisymmetric) states. Some examples of the symmetries of these edge modes are displayed in Figure 4 for $d_1 = 2$ cm (Figure 4a–d) and $d_1 = 13$ cm (Figure 4e–l). The pressure fields of the different modes are obtained from the transfer matrix method (see Supplementary Materials SM1).

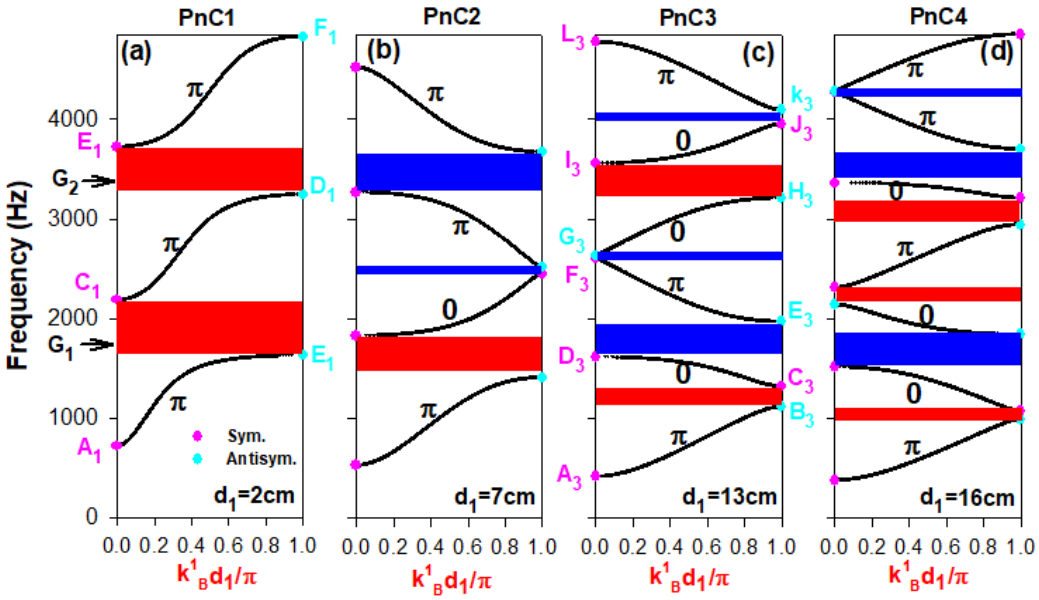

Figure 3. (**a**–**d**) Band structures for four infinite PnCs with different values of the period d_1 and $d_1' = 10$ cm. The Zak phases of each bulk band are labeled π or 0 in black. The pink (cyan) dots at the band edges represent the symmetric (antisymmetric) states. G1 and G2 indicate the position of the first and second common bandgaps. The bandgaps are colored in blue or red depending on whether the signs of the reflection phases of the semi-infinite PnCs are negative or positive.

Based on the above symmetry argument, we study the existence of a topological interface state in the common bandgaps for different combinations of the four PnCs 1 to 4. These crystals are indicated by dashed lines in Figure 2 and the symmetries of their band edge states are highlighted by cyan and pink colors. The corresponding dispersion curves and bandgaps are given in Figure 3. One can see that all bandgaps that can support interface states are of the hybridization type. Thus, for the combination PnC1+PnC2, there is no interface state in the lowest common bandgap around 1800 Hz, denoted G1 in Figure 3. Indeed, the lower (resp., upper) edge states of the corresponding gaps have the same symmetry, namely, they are both symmetric (resp., antisymmetric) as illustrated in Figure 2 and in Figure 4. In contrast, the higher common bandgap around 3400 Hz, denoted G2, supports an interface state because the lower (resp., upper) band edge states have opposite symmetries. A similar conclusion holds for the combinations PnC3+PnC4. The same symmetry argument allows us to conclude that for the combinations PnC1+PnC3 and PnC2+PnC4, there is one interface state in the lower common bandgap and no interface state in the higher common bandgap. Finally, the combinations PnC1+PnC4 and PnC2+PnC3 display an interface state in both common bandgaps. All these conclusions about the interface states in the common bandgaps G1 and G2 are summarized in Table 1.

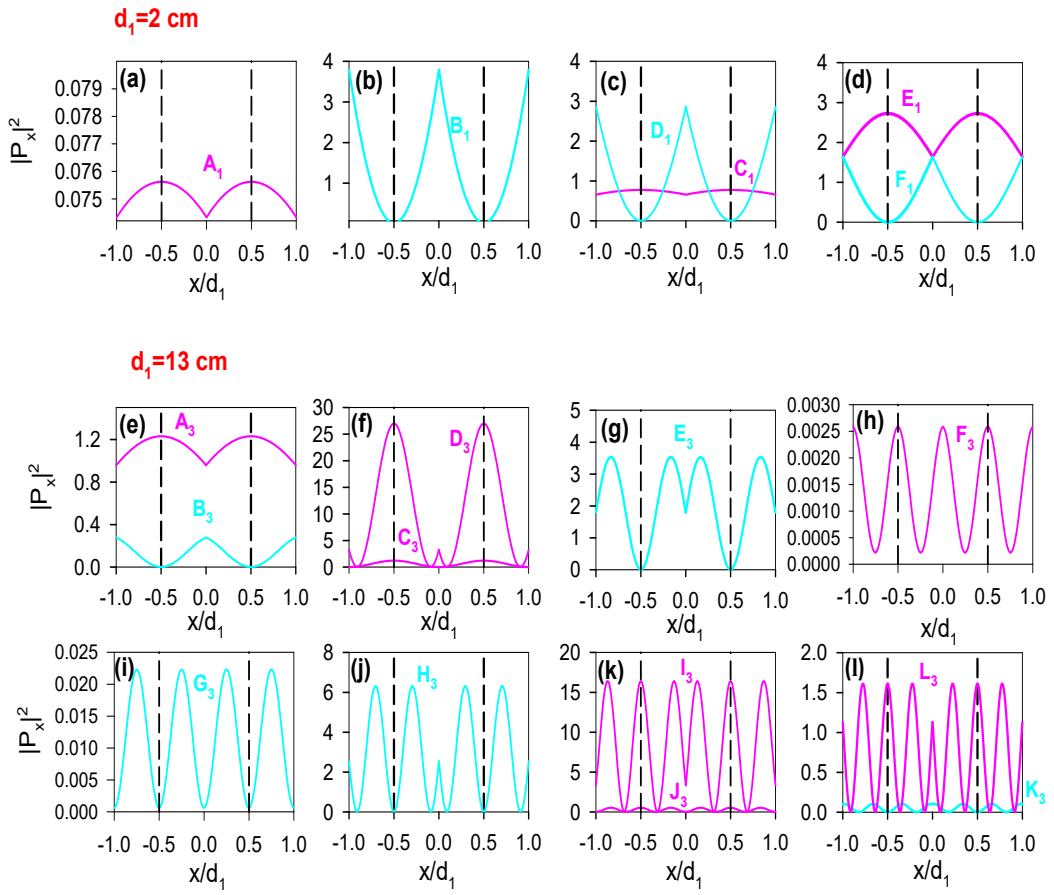

Figure 4. (**a**–**l**) Square modulus of the pressure field of different band edge states labeled A_1–L_3, respectively, for $d_1 = 2$ cm and $d_1 = 13$ cm. Pink and cyan colors indicate the symmetric and antisymmetric edge modes, respectively.

In addition, the sign of the reflection phases in the bandgaps can be deduced from the Zak phases of the bulk bands from the relation [26,32],

$$\mathrm{sgn}(\phi_n) = (-1)^{n+1} \exp\left(i \sum_{m=1}^{n-1} \theta_m^{\mathrm{Zak}} \right). \tag{3}$$

The sign of the reflection phases in the bandgaps of the four PnCs are plotted in Figure 3 in red and blue colors. The red and blue colors correspond to $sgn(\phi_n) > 0$ and $sgn(\phi_n) < 0$, respectively. Moreover, the existence of topological interface states can be predicted by the signs of the reflection phases in the bandgaps. A topological interface state can be obtained in the different configurations if the reflection phases of two PnCs take opposite signs, i.e., the colors in the common bandgaps are different. All these conclusions about the possibility of the existence of interface states based on the sign of the phase of the reflection coefficients for different configurations in Figure 3 are in accordance with those summarized in Table 1.

Table 1. The existence or nonexistence of topological interface states for different interface configurations constructed from the four PnCs in Figure 3.

PnCs	Common Bandgap G1	Common Bandgap G2
PnC1/PnC2	No	Yes
PnC1/PnC3	Yes	No
PnC1/PnC4	Yes	Yes
PnC2/PnC3	Yes	Yes
PnC2/PnC4	Yes	No
PnC3/PnC4	No	Yes

3. Interface States from Dispersion Relation and Local Density of States

In this section, we discuss the existence of interface states through the analysis of the dispersion relation of the semi-infinite PnCs and the local density of states (LDOS) at the interface point (labeled 0) between two semi-infinite comblike PnCs (Figure 1a). The acoustic interface states can be directly obtained through the dispersion relation of the semi-infinite PnCs (Figure 1a), namely, [3,52]

$$g^{-1}(\omega^2) = g_1^{-1}(\omega^2) + g_2^{-1}(\omega^2) = 0, \tag{4}$$

where $g_i(\omega^2)$ $(i = 1, 2)$ is the Green's function element at the surface of each PnC before their coupling. For open boundary conditions at the surface, its expression is given by [52]

$$g_i(\omega^2) = \frac{1}{\Delta_i}\left[\frac{S_i}{F} - \frac{S_i''}{FC_i''}(C_i - \frac{1}{t_i})\right], \tag{5}$$

where

$$\Delta_i = C_i - \frac{S_i S_i''}{C_i''} - \frac{1}{t_i}, \tag{6}$$

with $C_i'' = \cos(k\frac{d_i}{2})$, $S_i'' = -j\sin(k\frac{d_i}{2})$ $(i = 1, 2)$ and $F = \frac{-j\omega}{Z}$. The parameter t_i is defined as $t_i = \exp(k_B^i d_i)$, where d_i is the period of each PnC (Figure 1a,b) and k_B^i is the Bloch wavevector of each PnC given by Equation (1).

Now, we introduce the surface impedance Z_i of each semi-infinite PnC as follows

$$g_i^{-1}(\omega^2) = \frac{j\omega}{Z_i}(i = 1, 2). \tag{7}$$

From Equations (4) and (7), one can get easily

$$Z_1 + Z_2 = 0, \tag{8}$$

which is the well-known matching impedance condition [43] that should be satisfied in order to realize interface states between two media.

Moreover, the interface states can be revealed by the LDOS at the connection point (labeled 0) between the two PnCs (Figure 1a), which is given by [3,52],

$$n(\omega) = \frac{2\omega}{\pi} Im[g(\omega^2)] = \frac{2\omega}{\pi} Im\left[\frac{g_1(\omega^2)g_2(\omega^2)}{g_1(\omega^2) + g_2(\omega^2)}\right]. \tag{9}$$

Now, we discuss the common bandgaps between two semi-infinite PnCs and the existence of the interface state from the maxima of the LDOS at the junction point between the two crystals. For that purpose, let us fix the parameters $d_1 = 2$ cm, $d_1' = d_2' = 10$ cm and vary the parameter d_2. For each value of d_2, we can plot the projected band structures of both crystals 1 and 2 from Figure 2. Their superposition is shown in Figure 5a as a function of the parameter d_2 where the white areas represent the common bandgaps of the two

PnCs. The blue branches inside the gaps are the localized interface Tamm states obtained from the maxima of the LDOS (Equation (9)), as illustrated in Figure 5b for a few values of d_2. The dispersion curves of the interface states decrease when increasing d_2 and merge inside the bulk bands where they become resonant (leaky) modes. From Figure 5b, one can observe that for $d_2 = 10$ cm and 16 cm, there is an interface mode in each of the common bandgap, whereas at $d_2 = 13$ cm, the interface state exists only in the lower bandgap.

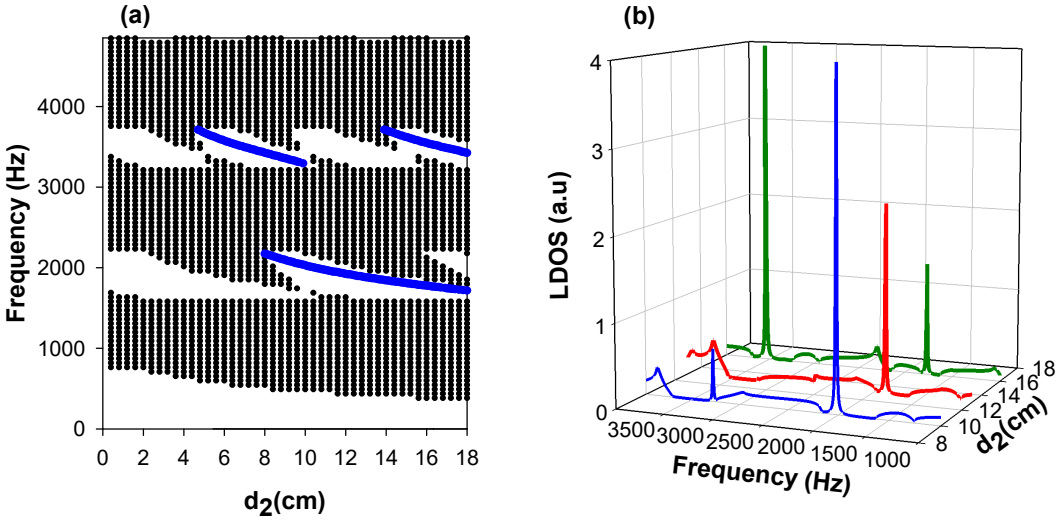

Figure 5. (**a**) Projected bandgap structure as a function of the period of the second PnC of length d_2 and a fixed period of the first PnC $d_1 = 2$ cm. The lengths of the stubs are assumed to be similar ($d_1' = d_2' = 10$ cm). Shaded areas represent bulk bands, while white areas display common bandgaps between the two PnCs. Blue branches represent interface Tamm states inside the common bandgaps obtained by the maxima of LDOS. (**b**) Examples of LDOS spectra as a function of frequency for three values of d_2: $d_2 = 10$ cm, $d_2 = 13$ cm and $d_2 = 16$ cm.

4. Interface States from Reflection Phases and Transmission Coefficient

In this section, we show the existence and the position of topological interface states in our phononic systems from the phases of the reflection coefficients at the boundary of each PnC with a waveguide (Figure 1b) or the transmission spectrum through two connected finite PnCs (Figure 1c).

The reflection coefficient r_i (i = 1, 2) is calculated separately between each PnC and a homogeneous waveguide characterized by impedance Z (i.e., $g^{-1}(\omega^2) = \frac{j\omega}{Z}$). Its expression is given by

$$r_i = \frac{Z_i - Z}{Z_i + Z} (i = 1, 2). \tag{10}$$

From Equation (10), one can deduce

$$Z_i = Z\left(\frac{1 - r_i}{1 + r_i}\right). \tag{11}$$

Equations (7) and (11) enable us to get $r_1 r_2 = 1$, which is equivalent to $|r_1||r_2| = 1$ and $\phi_{PnC1} + \phi_{PnC2} = 0$. In addition, from Equation (3), the Zak phase of a given bulk band can be obtained from the sign of the reflection phase in the bandgaps surrounding this band, namely, [26,42]

$$\exp(i\theta_n^{Zak}) = -\frac{\mathrm{sgn}(\phi_n)}{\mathrm{sgn}(\phi_{n-1})}, \tag{12}$$

where ϕ_n and ϕ_{n-1} are the reflection phases of the nth and $(n-1)$th bandgap, respectively. If the bandgaps have the same reflection phase sign (both positive or both negative), the

Zak phase is π, otherwise it is 0. This property has been exploited experimentally to deduce the Zak phases from the reflection phases [32].

Now, one can predict the existence and the position of the interface states through the reflection phases intersections, i.e., when the condition $\phi_{PnC1} + \phi_{PnC2} = 0$ is satisfied. In Figure 6a,b, we plot the reflection amplitudes and the corresponding phases for two PnCs made of the same material with different geometries: $d_1 = 2$ cm and $d_1' = 10$ cm (PnC1) and $d_2 = 13$ cm and $d_2' = 10$ cm (PnC3). The red (green) curves show the results for the first (second) PnC. The reflection amplitudes reach unity in the bandgap frequency regions. Based on the sign of the reflection phases, we have identified the Zak phases of each bulk band of the two PnCs. In addition, the position of the topological interface states can be obtained by the surface impedance condition $\phi_{PnC1} + \phi_{PnC3} = 0$ [26,32]. Indeed, the intersection between ϕ_{PnC1} (red curves) and $-\phi_{PnC3}$ (green curves) at $f = 1874.60$ Hz in the second common bandgap (G2) shows the position of the interface Tamm state (indicated by a blue filled circle at $f = 1874.60$ Hz). However, the signs of the phases in the second common bandgap G2 are similar and therefore such a gap cannot support an interface state. This result is also confirmed in the transmission spectra in Figure 6c when we consider two connected finite PnCs, each one made of N = 3 cells with different geometries (Figure 1c). Despite the small number of cells (N = 3), the transmission bandgap regions coincide well with those of the infinite crystal. The interface Tamm state (labeled T) appears as a transmission peak at $f = 1874.6$ Hz inside the first common bandgap G1 and coincides well with the interface state between two semi-infinite PnCs (indicated by a filled circle in Figure 6b). The intensity of the resonance reaches unity since the impedance adaptation at the interface between the two finite PnCs (i.e., no reflection at the interface) is respected.

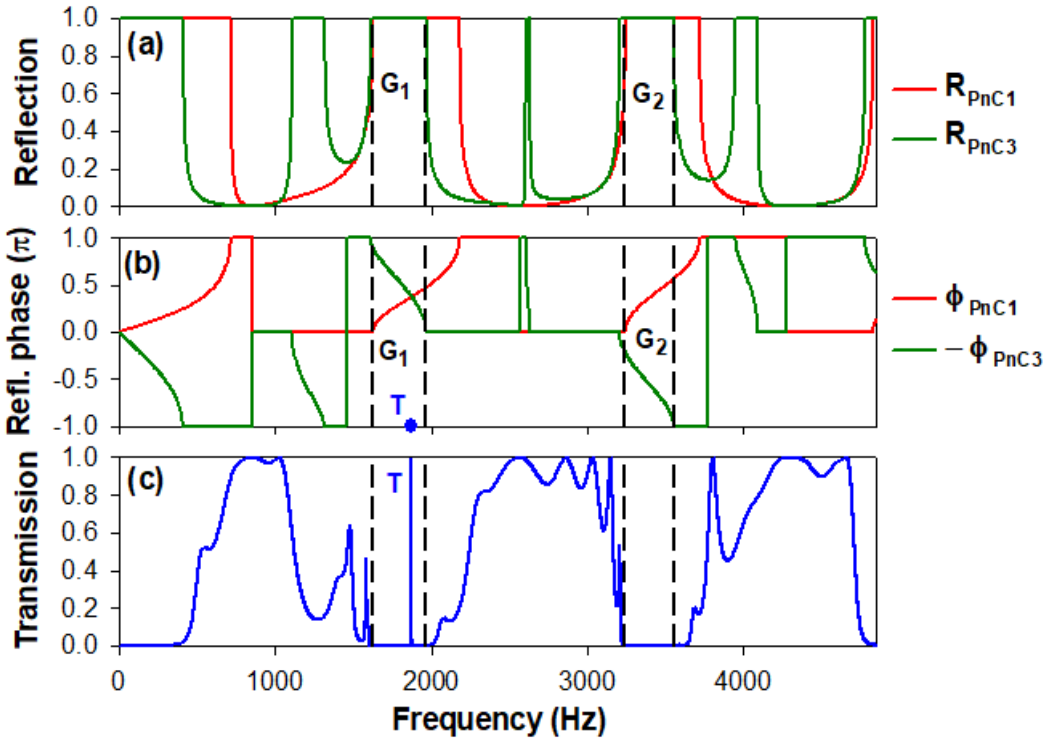

Figure 6. (**a**,**b**) Reflection amplitudes and the corresponding phases at the boundary of each PnC with the waveguide system (Figure 1b). The first PnC (PnC1) is made by stubs of length $d_1' = 10$ cm and period of length $d_1 = 2$ cm, while the second PnC (PnC3) is made by stubs of length $d_2' = 10$ cm and period of length $d_2 = 13$ cm. The blue dot in (b) indicates the position of the interface state. (**c**) Transmission coefficient for two finite connected PnCs, each one is made of N = 3 stubs (Figure 1c).

The behavior of the transmission as a function of the frequency for the six combinations listed in Table 1 is given in Figure 7. One can notice the existence of interface states in

the first and second common bandgaps labeled T and T', respectively. The existence of these modes for each pair of PnCs is in accordance with the predicted results in Table 1 and Figure 3. However, there exists a particular case (PnC2/PnC3) where the two predicted modes in the lower and upper bandgaps (see Table 1) do not appear in the transmission spectrum of Figure 7d. These modes belong to what is called BICs, which are characterized by a zero width, infinite lifetime or infinite quality factor [51]. Indeed, the position of the BIC can be obtained from vanishing the denominator of the transmission and reflection coefficients (see Equations (S.17)–(S.20) in the SM2). However, this quantity is complex and therefore the BIC is obtained from vanishing both its real and imaginary parts. After a tedious analytical calculation, we show that the BIC position is given by the geometrical parameters

$$\frac{d_1 + d_2}{d_1'} = \frac{2m}{n}, \tag{13}$$

and the frequency

$$f = \frac{mv}{2d_1'}, \tag{14}$$

where m and n are nonzero integers. This mode corresponds to stationary modes of the cavity of length $\frac{d_1+d_2}{2}$ surrounded by two stubs of length d_1' with a Dirichlet boundary condition at its extremities. This mode is independent of the number of cells N and the semi-infinite waveguides. Therefore, the BIC positions of the lower and upper modes in Figure 7d with $d_1 = 7$ cm and $d_1' = 10$ cm are given, respectively, by $m = n = 1$ in Equations (13) and (14) (i.e., $d_2 = 13$ cm and $f = 1710$ Hz) and $m = n = 2$ (i.e., $d_2 = 13$ cm and $f = 3420$ Hz). These two modes are indicated by vertical arrows in Figure 7d.

Figure 8a illustrates the shape and the width of the lower interface branch in Figure 5a in the transmission spectra for a fixed $d_1 = 2$ cm and a variable d_2 from 10 cm to 18 cm. One can see that for $d_2 = 10$ cm (red curve), the interface state appears as a Fano resonance [50] with an asymmetrical shape. When d_2 increases, the interface resonance becomes symmetric, its width decreases and its position shifts to lower frequencies. For $d_2 = 18$ cm, this resonance becomes a BIC with zero width at $f = 1710$ Hz (indicated by a blue arrow). Indeed, Equations (13) and (14) give exactly $d_2^{BIC} = 18$ cm and $f_{BIC} = 1710$ Hz for $m = n = 1$, $d_1 = 2$ cm and $d_1' = 10$ cm. The evolution of the transmission spectra (in color scale) as a function of d_2 and the frequency is given in Figure 8b. The interface state appears as a sharp branch resonance, its width decreases as d_2 increases and closes at $d_2^{BIC} = 18$ cm and $f_{BIC} = 1710$ Hz giving rise to the BIC. When d_2 tends to d_2^{BIC}, the width of the resonance goes to zero and therefore, the quality factor of theses modes diverges to infinity as illustrated in Figure 8c. Despite the small number of cells considered in each PnC in Figure 8b (N = 3 cells), the interface branch is very close to the one obtained in Figure 5a for two semi-infinite PnCs.

In order to check the robustness of the topological BIC against geometrical perturbations, we introduced a disorder in the system by changing the lengths of the stubs and periods for a finite system made of 10 cells. We kept the cavity of length $\frac{d_1+d_2}{2}$ and the two surrounding stubs of length d_1' unchanged and we introduced the disorder in the other lengths of the periods and stubs. To this end, we numerically implemented a disorder realization of strength δ ranging from zero (unperturbed system) to 0.1 (perturbed system). The lengths of the periods d_i $(i = 1, 2)$ were uniformly random in the interval $[d_i - \delta d_i, d_i + \delta d_i]$ $(i = 1, 2)$ and the lengths of the stubs d_i' $(i = 1, 2)$ were uniformly random in the interval $[d_i' - \delta d_i', d_i' + \delta d_i']$ $(i = 1, 2)$. For each strength of the perturbation, 10 different disorder realizations were considered. Figure 8d compares the effect of the disorder on the BIC (at $d_2^{BIC} = 18$ cm) and two other modes (labeled 1 and 2 in Figure 8b). As predicted, we can see that the BIC is much more robust to the disorder strength δ compared to the other two modes; this is because the BIC is a mode decoupled from the rest of the system and depends only on the cavity of length $\frac{d_1+d_2}{2}$ surrounded by two stubs of length d_1' with a vanishing pressure field at the connection points. As δ increases, the BIC stays pinned at the

same frequency $f_{BIC} = 1710$ Hz, whereas the other modes 1 and 2 fluctuate. In addition, one can notice that as d_2 goes away from d_2^{BIC}, the mode becomes more sensitive to the disorder strength.

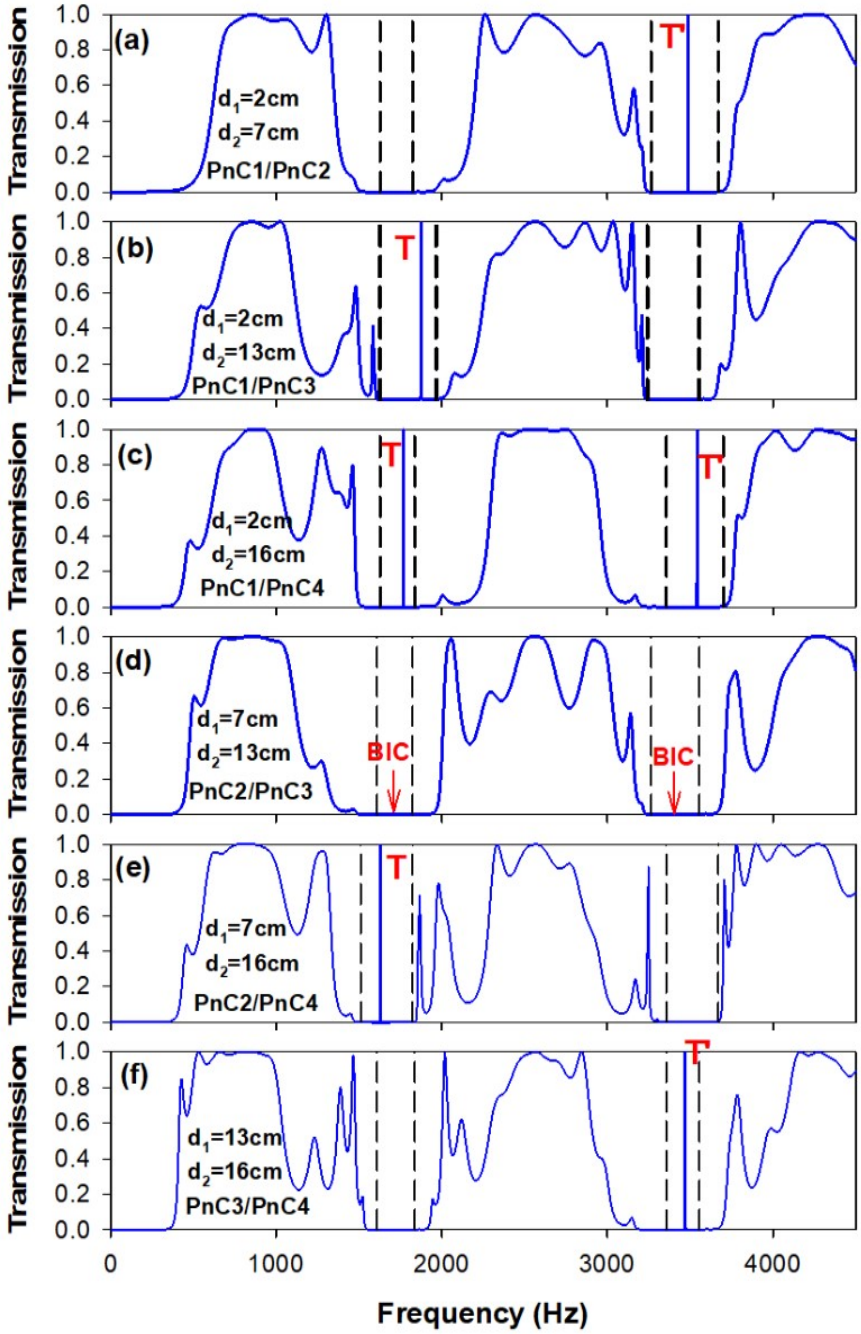

Figure 7. (**a**–**f**) Transmission spectra when two finite PnCs are connected together, each one made of N = 3 stubs (Figure 1c) for different combinations of PnCs pairs in Table 1, which are constructed from the four PnCs in Figure 3. The lengths of the stubs are fixed at $d_1' = d_2' = 10$ cm. T and T' indicate the positions of the acoustic interface states in the first and second common bandgaps, respectively.

In addition to the transmission coefficient, another interesting quantity can be used to deduce the existence of the interface states in the system such as the variation of the total density of states (DOS) of the whole structure and the phase of the determinant of the scattering matrix S ($det(S) = rr' - t^2$), the so called Friedel phase θ_F [56]. For a lossless system, one can show that the two quantities are related by the following expression (see SM2 for the details of the calculation) [57],

$$\frac{d\theta_F}{d\omega} = 2\pi\Delta n(\omega), \tag{15}$$

where $\Delta n(\omega)$ is the variation of the density of states between the finite PnC in Figure 1c and a reference system formed out of the two semi-infinite waveguides and the finite PnCs.

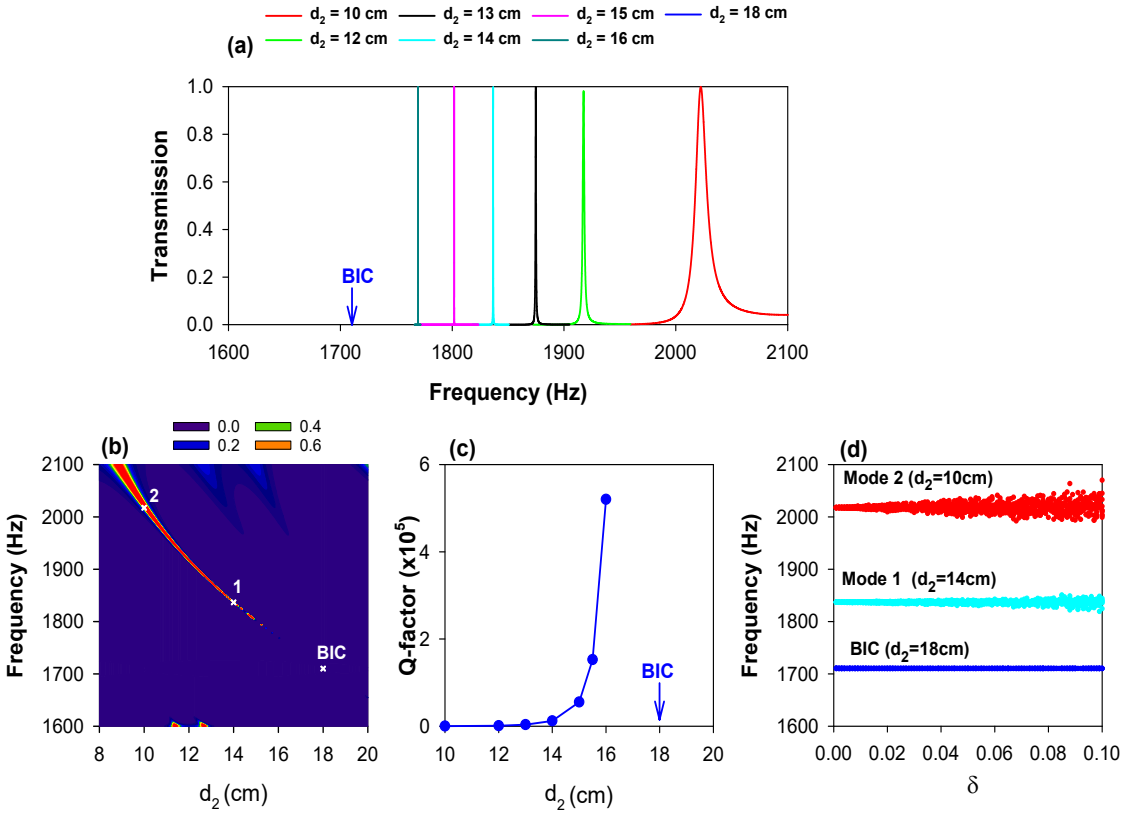

Figure 8. (**a**) Transmission spectra for certain values of d_2 around d_2^{BIC} and a fixed $d_1 = 2$ cm (PnC1). (**b**) Variation of the transmission coefficient as a function of d_2 and frequency in the first common bandgap. The crosses indicated by 1, 2 and BIC give the values of d_2 for which the effect of disorder is discussed in panel (**d**). (**c**) Quality factor of the interface states deduced from the width of the resonances in (**a**) as a function of d_2. (**d**) Evolution of the interface modes marked by crosses in panel (**b**) for 10 realizations of disorder by varying the disorder strength δ: BIC (blue curve), mode 1 (cyan curve) and mode 2 (red curve).

Figure 9a reproduces the transmission spectrum for $d_1 = 2$ cm and $d_2 = 13$ cm with $d_1' = d_2' = 10$ cm as discussed in Figure 7b. Figure 9b shows the variation of the DOS (red curves) as a function of frequency. The interface state appears as a well-defined peak inside the first common bandgap. The variation of the DOS gives a clear signature of the different interface states inside the bandgaps. Obviously, the phase of the determinant of the scattering matrix can be represented by the same curve based on the theoretical demonstration of Equation (15). It is worth noticing that the latter quantity has been measured experimentally in photonic circuits [57].

Let us mention that the interface modes can be affected by external perturbations, for instance by changing the temperature of the gas in the waveguides [58]. This effect is further discussed in SM3.

In order to show the effect of the tubes at the surface on the topological interface state, we plotted in Figure 10 the variation of interface state as a function of ϵ, where ϵ represents the detuning of the tubes at the surface from $\frac{d_1}{2} + \frac{d_2}{2}$ (i.e., $\epsilon = d_{s1} + d_{s2} - \frac{(d_1+d_2)}{2}$). The other tubes of the PnCs are fixed at $d_1 = 2$ cm (PnC1), $d_2 = 13$ cm (PnC3) and $d_1' = d_2' = 10$ cm.

One can see that the interface states appear as localized states inside the common bandgaps of the two PnCs (white areas); their positions depend on the variation of ϵ. Obviously, the interface state that appears at $\epsilon = 0$ (i.e., $d_{s1} = \frac{d_1}{2}$ and $d_{s2} = \frac{d_2}{2}$) strongly depends on the lengths ϵ and goes to lower frequencies as ϵ increases. Moreover, the interface states appear periodically as a function of ϵ.

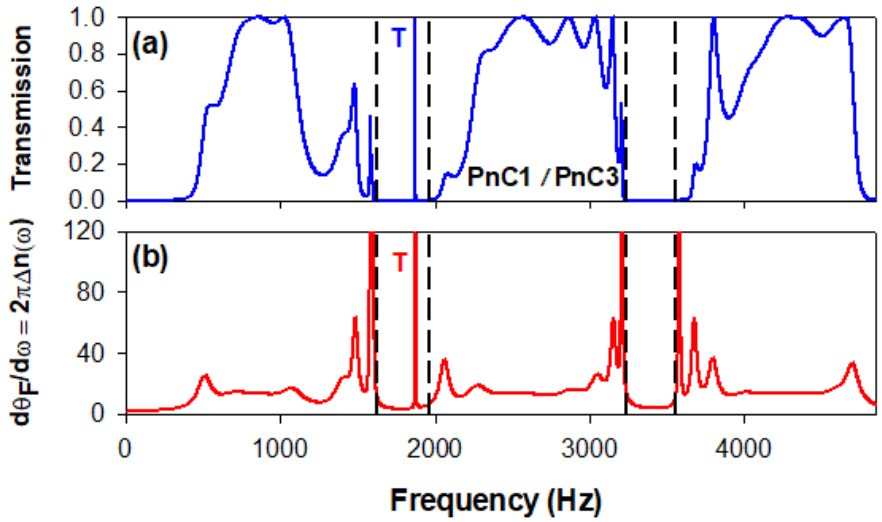

Figure 9. (**a**) Transmission coefficient for PnC1 and PnC3 with $d_1' = d_2' = 10$ cm. (**b**) Variation of the DOS as a function of frequency. The vertical dashed lines indicate the limits of the first and second common bandgaps.

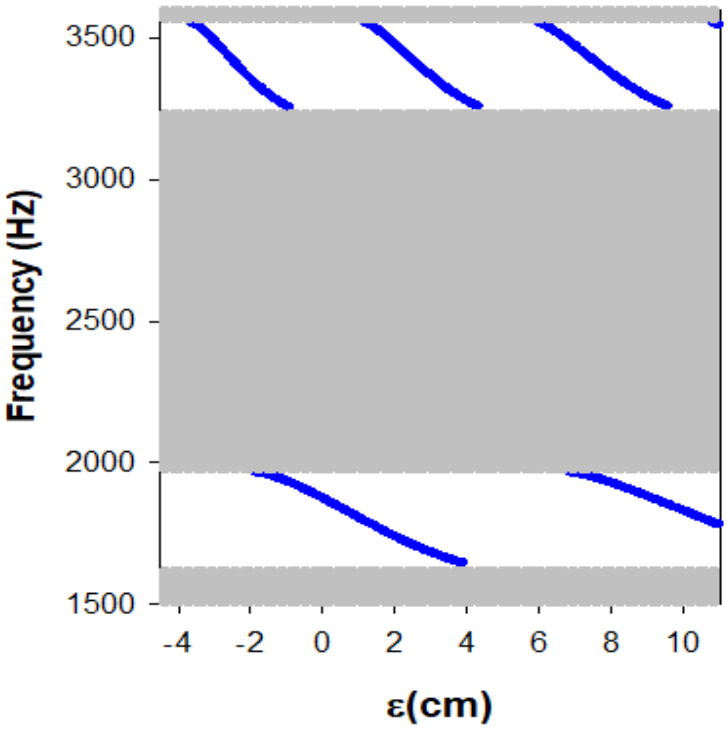

Figure 10. Interface states as function of ϵ for fixed values of the length of the stubs $d_1' = d_2' = 10$ cm and periods $d_1 = 2$ cm for PnC1 and $d_2 = 13$ cm for PnC3. ϵ represents the detuning of the tubes at the surface from $\frac{d_1}{2} + \frac{d_2}{2}$.

In addition to true localized interface states that fall inside the common bandgaps of two different PnCs, one can also obtain pseudointerface states (or semilocalized states)

which appear as resonances within the bandgap of one PnC and the bulk band of the other one. Figure 11a gives a zoom of the dispersion curves around the first common bandgap of two PnCs with $d_1 = 2$ cm (PnC1 with black curves) and $d_2 = 13$ cm (PnC3 with red curves). One can notice the existence of a region of frequency around 2100 Hz where the bandgap of PnC1 coincides with the bulk band of PnC3. In order to illustrate the behavior of the pseudointerface states, we plotted in Figure 11b,c the variation of the DOS as a function of frequency for $\epsilon = 0$ and $\epsilon = -2.5$ cm, respectively, around the common bandgap of the two PnCs. For $\epsilon = 0$ (i.e., the two tubes at the interface are fixed at $\frac{d_1}{2}$ and $\frac{d_2}{2}$), one obtains the topological interface state which falls inside the common bandgap of the two PnCs. By slightly changing ϵ from $\epsilon = 0$, the interface state moves inside the common bandgap until it merges within the bulk band of PnC3 (red curves) and becomes a resonant (leaky) mode for $\epsilon = -2.5$ cm (Figure 11c).

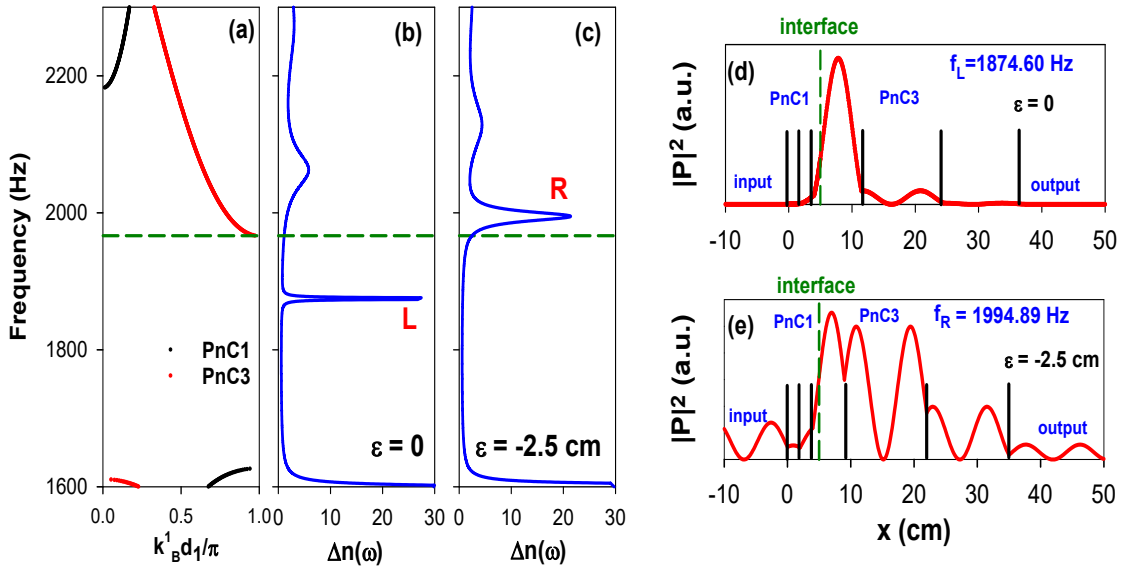

Figure 11. (**a**) Zoom of the dispersion curves for PnC1 with $d_1 = 2$ cm (black curves) and PnC3 with $d_1 = 13$ cm (red curves) around the first common bandgap G1. (**b**,**c**) Variation of the total DOS of a finite PnC composed of PnC1 ($d_1 = 2$ cm) and PnC3 ($d_2 = 13$ cm) for $\epsilon = 0$ (**b**) and $\epsilon = -2.5$ cm in Figure 10. Horizontal dashed line indicates the limit of the bandgap of PnC3. (**d**,**e**) Square modulus of the pressure field (in arbitrary units) versus the space position along the two combined PnCs for the localized and pseudointerface states at $f_L = 1874.60$ Hz and $f_R = 1994.89$ Hz in (**b**) and (**c**), respectively.

In order to show the spatial localization of the localized and pseudo interface states, we present in Figure 11d,e the distribution of the pressure field $|P|^2$ (in arbitrary units) as a function of the space position along the two combined PnCs at the frequency of the interface Tamm states in Figure 11b,c for $\epsilon = 0$ and $\epsilon = -2.5$ cm, respectively. For the localized Tamm state (labeled L in Figure 11b at $f_L = 1874.60$ Hz), one can observe that the pressure field of this state is strongly localized at the interface between the two PnCs located at $x = 5$ cm and decays rapidly in the bulk away from the interface. The main acoustic energy is localized in the first segment of length $\frac{d_2}{2}$ of the second PnC. However, for the pseudointerface state (labeled R in Figure 11c at $f_R = 1994.89$ Hz), the pressure field decreases rapidly from the interface inside the first PnC (on the left side), while it decreases less rapidly in the bulk of the second PnC (on the right side).

In all the previous sections, we fixed the lengths of the stubs at $d_1' = d_2' = 10$ cm to get interface states. Here, we discuss the possibility of the existence of interface states as a function of the lengths of the stubs for a fixed value of the period. To this end, we plot in Figure 12a the bandgap structure (white areas) of an infinite PnC as a function of the length d_1' for a fixed period $d_1 = 10$ cm. One can observe the existence of band

crossing points (labeled 1 to 6) where the bands close and reopen as function of d_1'. By slightly shifting from these points, one can obtain a common bandgap between two PnCs for different values of d_1'. The symmetry of the band edge states as a function of d_1' are shown by pink and cyan colors for symmetric and antisymmetric states, respectively. From the symmetry argument, one can obtain the Zak phases of the bulk bands such as zero or π depending on the value of d_1'. The areas where the Zak phase is π are indicated by a gray color, while the areas where the Zak phase is zero are indicated by a dark cyan color. Based on the symmetry of the band edge states, one can notice that it is impossible to get interface states in all common bandgaps for any two PnCs whatever the value of d_1', since their edge states are characterized by the same symmetry (i.e., both symmetric or both antisymmetric). For example, consider two PnCs with different values of d_1' such as $d_1' = 6$ cm and $d_1' = 12$ cm (PnCI and PnCII indicated by vertical dashed lines), one can obtain a common bandgap between these two PnCs (indicated by large circles); however, the symmetries of their lower (upper) band edges are similar, and therefore the common bandgap does not support an interface state. This result is also confirmed in the DOS and transmission spectra in Figure 12b,c, when we consider a finite PnC (Figure 1c) composed of two finite PnCs (PnCI and PnCII). One can see that there is no interface state signature inside the common bandgap (indicated by vertical dashed line) of the two PnCs.

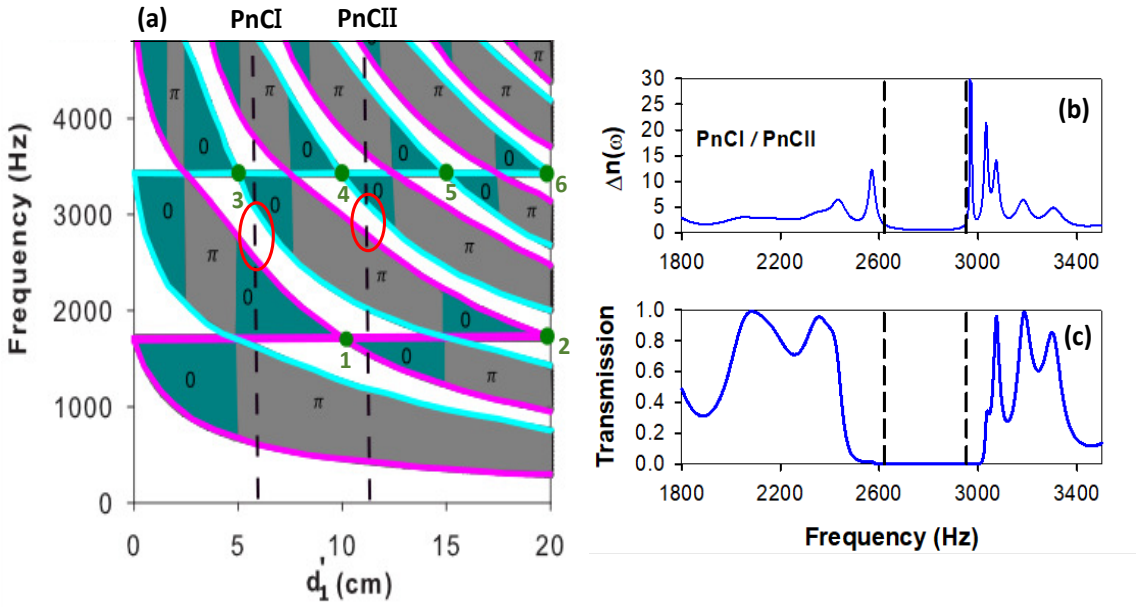

Figure 12. (**a**) Bandgaps (white area) separated by bands (shaded area) of an infinite PnC as a function of the length of the stub d_1', while the length of the period d_1 is fixed at 10 cm. The green circles labeled 1 to 6 indicate the positions of the band crossing points (where the dispersion curves become flat). The vertical dashed lines correspond to the two PnCs. Pink and cyan colors indicate the symmetric and antisymmetric edge modes of the common bandgaps, respectively. (**b**,**c**) DOS and transmission spectra for a finite PnC (Figure 1c) composed of two finite PnCs (PnCI and PnCII) with $d_1' = 6$ cm and $d_2' = 12$ cm and a fixed period $d_1 = d_2 = 10$ cm.

5. Conclusions

We investigated the existence of acoustic interface states between two topologically different PnCs. The PnCs were both 1D periodic comblike structures made of the same material but with different geometries. Contrary to the dimerized SSH model based on gapless bands with two stubs by cell, we proposed a new platform based on band closure (flat bands) and only one stub by unit cell. The tunability of common bandgaps and interface states was well discussed around the flat bands. First, we analyzed the possibility of the existence of interface states through an analysis of the band structure and the symmetry of the band edge states. This approach was equivalent to the analysis of the Zak phases of

the bulk bands of the two PnCs. The Zak phases of the bulk bands were determined using two approaches: (i) the symmetry of the band edge states and (ii) the sign of the reflection phases at the boundary of each PnC with a waveguide. Then, we showed that such interface states could be revealed by the LDOS which exhibited a high localization at the connection point between two semi-infinite PnCs. Moreover, the position of the interface state was deduced from the reflection-phase-matching condition $\phi_{PnC1} + \phi_{PnC2} = 0$. Furthermore, when two finite periodic systems were connected together, the Tamm states were revealed by sharp peaks in the transmission spectra. We demonstrated that the three methods supported each other and revealed the existence and the frequency position of the acoustic interface states. In addition to true localized interface states, we discussed the possibility of the existence of semilocalized interface states (i.e., interface resonances) that appear when the bandgap of one PnC coincides with the bulk band of the second one. In addition, we showed the possibility of the existence of topological BICs. These BICs were confined in the cavity separating both PnCs and remained very robust to any geometrical disorder induced by the stubs and segments around this cavity. Finally, we demonstrated that there was no interface state regardless of the lengths of the stubs between two different PnCs with similar periods. The calculations of the dispersion relations, DOS and scattering parameters were obtained by means of the Green's function method. The slender tubes used in this work could easily be extended to 1D side-coupled millimeter-scale Helmholtz resonators operating in the subwavelength domain [55], as well as to 2D topological PnCs [36,59,60]. In analogy with other waveguide devices, these results can be straightforwardly transposed to electromagnetic waves in photonic circuits with an experiment in the radiofrequency domain using standard coaxial cables [57] and to metal–insulator–metal (MIM) plasmonic nanostructures [22,61]. This work is in progress.

Supplementary Materials: The following supporting information can be downloaded at: https://www.mdpi.com/article/10.3390/cryst12121685/s1, title Supplementary material: Tunable Topological Acoustic Tamm States in Comblike Structures Based on Band Inversion around Flat Bands. The inverse of the Green's function of the stub of length $d_i^{'}$ in the space of interface $M_i^{'} = \{0, 0\}$ is given by [3,52].

Author Contributions: Investigation, S.K., Y.R., M.A., M.E.G. and E.H.E.B.; software, S.K., Y.R., M.A. and M.E.G.; supervision, E.H.E.B. and B.D.-R.; writing—original draft, S.K., Y.R., M.A. and M.E.G.; writing—review and editing, E.H.E.B., A.T. and B.D.-R. All authors have read and agreed to the published version of the manuscript.

Funding: This research received no external funding.

Institutional Review Board Statement: Not applicable.

Informed Consent Statement: Not applicable.

Data Availability Statement: Data available from the authors upon reasonable request.

Acknowledgments: The work of S. Khattou, Y. Rezzouk, M. Amrani and M. El Ghafiani was supported by the National Center of Scientific and Technical Research (CNRST) under the Excellence scholarship of Research.

Conflicts of Interest: The authors declare no conflict of interest.

References

1. Kushwaha, M.S.; Halevi, P.; Dobrzynski, L.; Djafari-Rouhani, B. Acoustic band structure of periodic elastic composites. *Phys. Rev. Lett.* **1993**, *71*, 2022. [CrossRef] [PubMed]
2. Khelif, A.; Adibi, A. (Eds.) *Phononic Crystals: Fundamentals and Applications*; Springer: Berlin, Germany, 2016.
3. Dobrzynski, L.; El Boudouti, E.H.; Akjouj, A.; Pennec, Y.; Al-Wahsh, H.; Lévêque, G.; Djafari, R.B. *Phononics*; Elsevier: Amsterdam, The Netherlands, 2017.
4. Yablonovitch, E. Inhibited spontaneous emission in solid-state physics and electronics. *Phys. Rev. Lett.* **1987**, *58*, 2059. [CrossRef] [PubMed]
5. Kushwaha, M.S.; Akjouj, A.; Djafari-Rouhani, B.; Dobrzynski, L.; Vasseur, J.O. Acoustic spectral gaps and discrete transmisson in slender tubes. *Solid State Commun.* **1998**, *106*, 659–663. [CrossRef]

6. El Boudouti, E.H.; Mrabti, T.; Al-Wahsh, H.; Djafari-Rouhani, B.; Akjouj, A.; Dobrzynski, L. Transmission gaps and Fano resonances in an acoustic waveguide: Analytical model. *J. Phys. Condens. Matter* **2008**, *20*, 255212. [CrossRef]
7. Narayanaamurti, V. Phonon optics and phonon propagation in semiconductors. *Science* **1981**, *213*, 717–723. [CrossRef]
8. Lee, S.H.; Park, C.M.; Seo, Y.M.; Wang, Z.G.; Kim, C.K. Acoustic metamaterial with negative modulus. *J. Phys. Condens. Matter* **2009**, *21*, 175704. [CrossRef]
9. Fang, N.; Xi, D.; Xu, J.; Ambati, M.; Srituravanich, W.; Sun, C.; Zhang, X. Ultrasonic metamaterials with negative modulus. *Nat. Mater.* **2006**, *5*, 452–456. [CrossRef]
10. Mouadili, A.; El Boudouti, E.H.; Djafari-Rouhani, B. Acoustic demultiplexer based on Fano and induced transparency resonances in slender tubes. *Eur. Phys. J. Appl. Phys.* **2020**, *90*, 10902. [CrossRef]
11. Wang, Z.G.; Lee, S.H.; Kim, C.K.; Park, C.M.; Nahm, K.; Nikitov, S.A. Acoustic wave propagation in one-dimensional phononic crystals containing Helmholtz resonators. *J. Appl. Phys.* **2008**, *103*, 064907. [CrossRef]
12. Robertson, W.M.; Ash, J.; McGaugh, J.M. Breaking the sound barrier: Tunneling of acoustic waves through the forbidden transmission region of a one-dimensional acoustic band gap array. *Am. J. Phys.* **2002**, *70*, 689–693. [CrossRef]
13. Akjouj, A.; Al-Wahsh, H.; Sylla, B.; Djafari-Rouhani, B.; Dobrzynski, L. Stopping and filtering waves in phononic circuits. *J. Phys. Condens. Matter* **2003**, *16*, 37. [CrossRef]
14. Munday, J.N.; Bennett, C.B.; Robertson, W.M. Band gaps and defect modes in periodically structured waveguides. *J. Acoust. Soc.* **2002**, *112*, 1353–1358. [CrossRef] [PubMed]
15. Tamm, I.Y. Rukovoyashchie idei v tvorchestve Faradeya. *Phys. Z. Sowjetunion* **1932**, *1*, 733.
16. El Hassouani, Y.; El Boudouti, E.H.; Djafari-Rouhani, B.; Aynaou, H.; Dobrzynski, L. Surface and interface acoustic waves in solid-fluid superlattices: Green's function approach. *Phys. Rev. B* **2006**, *74*, 144306. [CrossRef]
17. Mei, X.; Ke, M.; He, Z.; Yu, Z.; Yu, L.; Liu, Z. Acoustic Tamm states in double 1D phononic crystals. *J. Wuhan Univ. Technol. Mater.* **2012**, *27*, 374–376. [CrossRef]
18. Khattou, S.; Amrani, M.; Mouadili, A.; Djafari-Rouhani, B. Acoustic Tamm states in slender tubes. *Mater. Today Proc.* **2021**, *45*, 7394–7398. [CrossRef]
19. Djafari-Rouhani, B.; El Boudouti, E.H.; Akjouj, A.; Dobrzynski, L.; Vasseur, J.O.; Mir, A.; Fettouhi, N.; Zemmouri, J. Surface states in one-dimensional photonic band gap structures. *Vacuum* **2001**, *63*, 177–183. [CrossRef]
20. Liu, X.X.; Tsai, C.F.; Chern, R.L.; Tsai, D.P. Dispersion mechanism of surface magnetoplasmons in periodic layered structures. *Appl. Opt.* **2009**, *48*, 3102–3107. [CrossRef]
21. El Abouti, O.; El Boudouti, E.H.; El Hassouani, Y.; Noual, A.; Djafari-Rouhani, B. Optical Tamm states in one-dimensional superconducting photonic crystal. *Phys. Plasmas* **2016**, *23*, 082115. [CrossRef]
22. Rezzouk, Y.; Amrani, M.; Khattou, S.; Djafari-Rouhani, B. Plasmonic Tamm states in periodic stubbed MIM waveguides: Analytical and numerical study. *J. Opt. Soc. Am. B* **2022**, *39*, 600–610. [CrossRef]
23. Liu, F.; Wakabayashi, K. Novel topological phase with a zero berry curvature. *Phys. Rev. Lett.* **2017**, *118*, 076803. [CrossRef] [PubMed]
24. Xiao, D.; Chang, M.; Niu, Q. Berry Phase Effects on Electronic Properties. *Rev. Mod. Phys.* **2010**, *82*, 1959–2007. [CrossRef]
25. Zak, J. Berry's phase for energy bands in solids. *Phys. Rev. Lett.* **1979**, *62*, 1989. [CrossRef]
26. Xiao, M.; Zhang, Z.Q.; Chan, C.T. Surface impedance and bulk band geometric phases in one-dimensional systems. *Phys. Rev. X* **2014**, *4*, 021017. [CrossRef]
27. Xiao, M.; Ma, G.; Yang, Z.; Sheng, P.; Zhang, Z.Q.; Chan, C.T. Geometric phase and band inversion in periodic acoustic systems. *Nat. Phys.* **2015**, *11*, 240–244. [CrossRef]
28. Atala, M.; Aidelsburger, M.; Barreiro, J.T.; Abanin, D.; Kitagawa, T.; Demler, E.; Bloch, I. Direct measurement of the Zak phase in topological Bloch bands. *Nat. Phys.* **2013**, *9*, 795–800. [CrossRef]
29. Zhu, W.; Ding, Y.Q.; Ren, J.; Sun, Y.; Li, Y.; Jiang, H.; Chen, H. Zak phase and band inversion in dimerized one-dimensional locally resonant metamaterials. *Phys. Rev. B* **2018**, *97*, 195307. [CrossRef]
30. Wang, Q.; Xiao, M.; Liu, H.; Zhu, S.; Chan, C.T. Measurement of the Zak phase of photonic bands through the interface states of a metasurface/photonic crystal. *Phys. Rev. B* **2016**, *93*, 041415. [CrossRef]
31. Belozorov, D.P.; Girich, A.; Nedukh, S.V.; Moskaltsova, A.N.; Tarapov, S.I. Microwave analogue of Tamm states in periodic chain-like structures. *Prog. Electromagn. Res. Lett.* **2014**, *46*, 7–12. [CrossRef]
32. Gao, W.S.; Xiao, M.; Chan, C.T.; Tam, W.Y. Determination of Zak phase by reflection phase in 1D photonic crystals. *Opt. Lett.* **2015**, *40*, 5259–5262. [CrossRef]
33. Chen, Z.; Han, P.; Leung, C.W.; Wang, Y.; Hu, M.; Chen, Y. Study of optical Tamm states based on the phase properties of one-dimensional photonic crystals. *Opt. Express* **2012**, *20*, 21618–21626. [CrossRef] [PubMed]
34. Elshahat, S.; Mohamed, Z.E.A.; Almokhtar, M.; Lu, C. High tunability and sensitivity of 1D topological photonic crystal heterostructure. *J. Opt.* **2022**, *24*, 035004. [CrossRef]
35. Wang, L.; Cai, W.; Bie, M.; Zhang, X.; Xu, J. Zak phase and topological plasmonic Tamm states in one-dimensional plasmonic crystals. *Opt. Express* **2018**, *26*, 28963–28975. [CrossRef] [PubMed]
36. Ma, G.; Xiao, M.; Chan, C.T. Topological phases in acoustic and mechanical systems. *Nat. Rev. Phys.* **2019**, *1*, 281–294. [CrossRef]
37. Liao, D.; Yue, Z.; Zhang, Z.; Wang, H.X.; Cheng, Y.; Liu, X. Observations of Tamm modes in acoustic topological insulators. *Appl. Phys. Lett.* **2022**, *120*, 211701. [CrossRef]

38. Ortiz, O.; Priya, P.; Rodriguez, A.; Lemaitre, A.; Esmann, M.; Lanzillotti-Kimura, N.D. Topological optical and phononic interface mode by simultaneous band inversion. *Optica* **2021**, *8*, 598–605. [CrossRef]
39. Chen, Z.G.; Wu, Y. Tunable topological phononic crystals. *Phys. Rev. Appl.* **2016**, *5*, 054021. [CrossRef]
40. Fan, L.; Yu, W.W.; Zhang, S.Y.; Zhang, H.; Ding, J. Zak phases and band properties in acoustic metamaterials with negative modulus or negative density. *Phys. Rev. B* **2016**, *94*, 174307. [CrossRef]
41. Zhang, Z.; Cheng, Y.; Liu, X.; Christensen, J. Subwavelength multiple topological interface states in one-dimensional labyrinthine acoustic metamaterials. *Phys. Rev. B* **2019**, *99*, 224104. [CrossRef]
42. Li, Z.W.; Fang, X.S.; Liang, B.; Li, Y.; Cheng, J.C. Topological interface states in the low-frequency band gap of one-dimensional phononic crystals. *Phys. Rev. Appl.* **2020**, *14*, 054028. [CrossRef]
43. Meng, Y.; Wu, X.; Zhang, R.Y.; Li, X.; Hu, P.; Ge, L.; Huang, Y.; Xiang, H.; Han, D.; Wang, S.; et al. Designing topological interface states in phononic crystals based on the full phase diagrams. *Nat. J. Phys. Phys. Rev. B* **2018**, *20*, 073032. [CrossRef]
44. To, A.C.; Lee, B.J. Multifunctional One-Dimensional Phononic Crystal Structures Exploiting Interfacial Acoustic Waves. *MRS Online Proc. Libr. (OPL)* **2009**, *1188*, 145–149. [CrossRef]
45. Zheng, Z.; Yin, J.; Wen, J.; Yu, D. Multiple topological interface states in broadband locally resonant phononic crystals. *J. Appl. Phys.* **2021**, *129*, 184901. [CrossRef]
46. Su, W.; Schrieffer, J.R.; Heeger, A.J. Solitons in polyacetylene. *Phys. Rev. Lett.* **1979**, *42*, 1698. [CrossRef]
47. Meier, E.J.; An, F.A.; Gadway, B. Observation of the topological soliton state in the Su–Schrieffer–Heeger model. *Nat. Commun.* **2016**, *7*, 13986. [CrossRef] [PubMed]
48. Coutant, A.; Sivadon, A.; Zheng, L.; Achilleos, V.; Richoux, O.; Theocharis, G.; Pagneux, V. Acoustic Su-Schrieffer-Heeger lattice: Direct mapping of acoustic waveguides to the Su-Schrieffer-Heeger model. *Phys. Rev. B* **2021**, *103*, 224309. [CrossRef]
49. Cáceres-Aravena, G.; Real, B.; Guzmán-Silva, D.; Amo, A.; Torres, L.E.F.; Vicencio, R.A. Experimental observation of edge states in SSH-Stub photonic lattices. *Phys. Rev. Res.* **2022**, *4*, 013185. [CrossRef]
50. Fano, U. Effects of configuration interaction on intensities and phase shifts. *Phys. Rev.* **1961**, *124*, 1866. [CrossRef]
51. Hsu, C.W.; Zhen, B.; Stone, A.D.; Joannopoulos, J.D.; Soljačić, M. Bound states in the continuum. *Nat. Rev. Mater.* **2016**, *1*, 16048. [CrossRef]
52. Vasseur, J.O.; Akjouj, A.; Dobrzynski, L.; Djafari-Rouhani, B.; El Boudouti, E.H. Photon, electron, magnon, phonon and plasmon mono-mode circuits. *Surf. Sci. Rep.* **2004**, *54*, 1–156. [CrossRef]
53. Robertson, W.M.; Vazquez, C.; Lopez, J.; LaVerde, A.; Giuntini, R.J. Acoustic waveguide demultiplexer based on Fano resonance: Experiment and simulation. *AIP Adv.* **2022**, *12*, 045018. [CrossRef]
54. Merkel, A.; Theocharis, G.; Richoux, O.; Romero-Garcia, V.; Pagneux, V. Control of acoustic absorption in one-dimensional scattering by resonant scatterers. *Appl. Phys. Lett.* **2015**, *107*, 244102. [CrossRef]
55. Gu, T.; Cheng, Y.; Wen, Z.; Boudouti, E.H.E.; Jin, Y.; Li, Y.; Djafari-Rouhani, B. Induced transparency based subwavelength acoustic demultiplexers. *J. Phy. D Appl. Phys* **2021**, *54*, 175301. [CrossRef]
56. Friedel, J. The distribution of electrons round impurities in monovalent metals. *Lond. Edinb. Dublin Philos. Mag. J. Sci.* **1952**, *43*, 153–189. [CrossRef]
57. Khattou, S.; Amrani, M.; Mouadili, A.; Talbi, A.; Akjouj, A.; Djafari-Rouhani, B. Comparison of density of states and scattering parameters in coaxial photonic crystals: Theory and experiment. *Phys. Rev. B* **2020**, *102*, 165310. [CrossRef]
58. Kinsler, L.E.; Frey, A.R.; Coppens, A.B.; Sanders, J.V. *Fundamentals of Acoustics*; John Wiley and Sons: New York, NY, USA, 2000.
59. Ma, T.X.; Fan, Q.S.; Zhang, C.; Wang, Y.S. Acoustic flatbands in phononic crystal defect lattices. *J. Appl. Phys.* **2021**, *129*, 145104. [CrossRef]
60. Zhang, X.; Xiao, M.; Cheng, Y.; Lu, M.H.; Christensen, J. Topological sound. *Commun. Phys.* **2018**, *1*, 97. [CrossRef]
61. Khattou, S.; Amrani, M.; Mouadili, A.; El Boudouti, E.H.; Talbi, A.; Akjouj, A.; Djafari-Rouhani, B. Three port photonic and plasmonic demultiplexers based on Cross and U-shaped stub structures: Application for filtering and sensing. *J. Appl. Phys.* **2022**, *131*, 153102. [CrossRef]